NASA
Technical
Paper
2308

May 1984

Effects of Simulated Flight on the Structure and Noise of Underexpanded Jets

Thomas D. Norum
and John G. Shearin

NASA

NASA Technical Paper 2308

1984

Effects of Simulated Flight on the Structure and Noise of Underexpanded Jets

Thomas D. Norum
and John G. Shearin

Langley Research Center
Hampton, Virginia

NASA
National Aeronautics
and Space Administration

Scientific and Technical Information Branch

INTRODUCTION

The noise emitted from a supersonic jet has been the subject of numerous investigations over the past few decades. Research on this topic reached its peak in the 1970's with the construction of the Concorde in Europe and the planning for a supersonic transport in this country. The demise of the latter project was due in no small part to the inability to effect a quiet propulsion system. The resultant departure of researchers from this area has left a number of unsolved problems relevant to present and future needs. One concern is that commercial aircraft can have supersonic exhausts when cruising at altitude. The noise emitted from these exhausts may cause structural fatigue. Also, since military fighters are now capable of attaining supersonic nozzle pressure ratios statically as well as in flight, they have the additional problems associated with high noise levels at ground level.

The mixing of any jet with the medium into which it exhausts creates jet mixing noise. If the static pressure at the nozzle exit does not match the ambient pressure, shocks occur in the jet plume and additional noise can be created. This shock-associated noise has two identifiable components. The first is a set of discrete tones called screech, which was first studied in the early 1950's by Powell (ref. 1). Many investigations followed, a summary of which can be found in reference 2. The other component of shock-associated noise is called broadband shock noise, which Harper-Bourne and Fisher (ref. 3) semiempirically predicted in 1973. Here again, additional studies (refs. 4 and 5) have yielded an extensive data base for this component of supersonic jet noise.

Although many studies of the effects of forward motion on jet noise have been pursued, only a handful have involved supersonic jets. These include flight tests of subsonic aircraft attaining supersonic exhausts at altitude (ref. 6) and a few supersonic conditions tested on the Bertin Aérotrain (ref. 7). Bryce and Pinker (ref. 8) conducted a detailed study of flight simulation using a model-scale nozzle and a free jet. Their acoustic measurements were accompanied by shadowgraph visualization of the jet. Sarohia (ref. 9) attained higher free jet velocities with a similar experimental setup and found some surprising changes in the measured noise levels.

The objective of the current report is to relate changes in the radiated sound field of an underexpanded jet in forward motion to changes in the mean flow field. Far-field acoustic pressures and mean static and pitot plume pressures were measured over a wide range of nozzle exit conditions with and without external flow.

SYMBOLS

c_a ambient sound speed

c_j sound speed in fully expanded model jet

d model nozzle diameter

L	typical shock cell spacing
$\bar{L}_7$	average length of first seven shock cells
m	flight-effect directivity exponent of jet mixing noise
M_c	convection Mach number, U_c/c_a
M_f	flight Mach number, U_f/c_a
M_j	Mach number in fully expanded model jet, U_j/c_j
OASPL	overall sound pressure level
p_a	ambient static pressure
p_p	plume pitot pressure
p_s	plume static pressure
p_t	model jet stagnation pressure
r	radial distance from model jet centerline
r_f	radius of free jet
r_m	radius of microphone arc
r_s	radial extent of sonic line
SPL	sound pressure level, dB (re 20 μPa)
T	period of fundamental screech frequency or peak broadband shock noise frequency
U_c	average flow disturbance convection velocity
U_f	simulated flight velocity
U_j	velocity in fully expanded model jet
x	axial distance from model nozzle exit
x_s	distance from center of microphone arc to acoustic source
α	ratio of convection velocity to fully expanded velocity, U_c/U_j
β	shock parameter, $(M_j^2 - 1)^{1/2}$
θ	propagation angle inside free jet (figs. 21 and 22)
λ	wavelength of fundamental screech tone or peak broadband shock noise
λ_f	wavelength at the flight condition (U_f = 170 fps)

λ_o wavelength at the static condition ($U_f = 0$)

ϕ propagation angle outside free jet (fig. 22)

ψ far-field microphone angle measured from the upstream jet axis (fig. 2)

TEST DESCRIPTION

The test was conducted in the quiet flow facility in the Langley Noise Reduction Laboratory. This facility consists of an anechoic chamber with the capability of supplying high pressure air to a model jet nozzle and low pressure, high volume air to a free jet nozzle. The free jet surrounds the model jet to simulate the external flow in forward flight, as shown in figure 1. The chamber is approximately 20 ft × 24 ft × 30 ft and is lined with foam wedges to provide a cutoff frequency of about 70 Hz. Details of this facility can be found in reference 10.

The contoured, convergent sonic model nozzle had an exit diameter of 1 inch. To provide an unobstructed path to the most upstream microphone, the model nozzle exit was located 14 inches downstream from the exit of the 18-inch-diameter free jet nozzle. Twelve 1/4-inch microphones were located on an arc of 72-inch radius, centered on the axis of the sonic nozzle and 4 inches downstream from its exit. The microphones were positioned every 10° from 40° to 150° from the upstream axis. A sketch of the acoustic experimental setup is given in figure 2.

The model jet operating condition will be represented by the shock parameter β, which is related to the nozzle pressure ratio by

$$\beta^2 = M_j^2 - 1 = 5(p_t/p_a)^{2/7} - 6$$

Tests were conducted between the sonic condition ($\beta = 0$) and a highly underexpanded condition ($\beta = 1.8$). The stagnation pressure of the model jet was continuously monitored to ensure that deviations in the supply pressure never exceeded gage accuracy (± 0.25 psi). Free jet velocities ranged from 0 up to 170 fps (a Mach number of about 0.15). Unless otherwise stated, the data presented in this report were obtained at the free jet velocities of 0 and 170 fps, hereafter referred to as the static and flight conditions, respectively.

For the aerodynamic measurements, the floor wedges were removed and a three-dimensional traverse installed. Supersonic total and static pressure probes were alternately traversed through the model jet plume. The probe was positioned at 0.05-inch increments in the axial direction and 0.025-inch increments in the radial direction between successive data points. Probe positioning was sufficiently precise to ensure repeatability of the pressure surveys. The static probe is identical to that used in previous investigations and is described in detail in reference 5.

AERODYNAMIC RESULTS

Mean pitot and static pressures in the model jet plume were measured for simulated forward speeds of 0 and 170 fps. Data consistency was checked by comparing measured pressure profiles at the static condition with those obtained by Norum and Seiner (ref. 5) with a larger diameter nozzle. An example of such comparison is

given in figure 3, which shows the centerline static pressure distribution along with shock cell numbers at $\beta = 1.0$. Except for the magnitude of the expansion in the fifth and sixth shock cells, the two profiles agree very well at the same normalized axial location.

Figure 4 presents static pressure profiles measured along the jet centerline at $\beta = 0.60$, 0.94, and 1.50. Since only small differences exist between the profiles measured at the static and flight conditions at the lower values of β, only the flight data are presented. At $\beta = 1.50$, however, the effect of forward speed is more pronounced, so both static and flight profiles are given in figure 4(c). Although the two profiles are identical close to the nozzle exit, the flight profile is stretched further downstream, so that the downstream shock cells are longer. Changes in the extent of this stretching is illustrated in figure 5. In this figure, the axial locations of the static pressure maxima at the end of each shock cell are plotted against cell number for $\beta = 0.60$, 0.94, and 1.50. Flight has no influence on the positions of the closely spaced shocks at $\beta = 0.60$, with 11 shock cells occurring within the first 7 model jet diameters downstream. On the other hand, at about seven diameters downstream, noticeable stretching begins to occur at higher values of β. Further downstream, the shock spacings in flight are increased over the corresponding spacings at the static condition. Flight does not seem to influence the strength of these shocks, defined as the rise in static pressure within the shock cell divided by the minimum pressure. This can be seen in figure 6, in which static and flight shock strengths differ very little.

Hence at all values of β, the shock cell development along the jet centerline is unaffected by low flight speed in the initial region of the jet. The influence of flight is felt only after about seven diameters from the nozzle exit. Thereafter, there is a noticeable increase in the axial locations of the corresponding shocks although almost no change in their strengths.

Figures 5 and 6 also show that at least 11 shock cells exist at both the low and the high values of β, with the shock strengths gradually decreasing with cell number. At $\beta = 0.94$, however, only seven cells exist, and a drastic reduction in strength occurs between the third and fifth cells. This seemingly inconsistent behavior is examined more closely in figure 7, which gives the shock strengths of the first 10 cells measured along the jet centerline at the static condition. The strength of the first cell, shown as the dashed line, is strongly influenced by the nozzle internal expansion. After the first cell, the shock strengths decrease consistently with cell number at all values of β. Note that less than 10 cells exist in the range of β from 0.7 to 1.3, with the number of cells being a minimum in the neighborhood of $\beta = 0.9$.

A similar plot of shock strength measured near the nozzle lip line at a radial location $r/d = 0.45$ is given in figure 8. At high values of β, the first shock is very strong (note the scale change), corresponding to the existence of a Mach disc. The remaining shocks level off in strength, as has been discussed in reference 11. Since near the lip line the jet mixes with the surrounding air immediately upon exhaust, the dynamic pressure at low values of β is quickly reduced to a subsonic value, and hence only a few shocks can exist at this radial location. At higher values of β, considerably greater mixing is necessary to make the flow at the lip line subsonic, so that a larger number of shocks can exist. Hence, we can see that the existence of more shocks along the jet centerline at low values of β than at intermediate values can be attributed to the fact that the cells are so closely packed together at low values. Since mixing does not reach the jet axis within the

first few nozzle diameters from the exit, at low values of β the shocks decay before they can be influenced by the mixing.

Confirmation of this reason for fewer shocks along the jet centerline at the intermediate values of β was obtained from radial Mach number profiles at $\beta = 0.94$. These profiles were computed from radial distributions of static and pitot pressures at a number of axial locations. The variation of the sonic line (the projection of the surface within which supersonic flow exists) was then determined and plotted in figure 9. The initial jet expansion results in a 10-percent increase in the sonic line radius at a downstream distance of about one-half nozzle diameter. However, this is the maximum radial excursion of the sonic line; by six diameters from the nozzle exit, the sonic line has receded within the lip line and appears to be quickly headed toward the jet centerline. This quick reduction in the radial extent of the shock cells necessitates a corresponding reduction in the strength of the compression-expansion process and precludes shocks further downstream. The fast convergence of the sonic line at this condition is in sharp contrast to its behavior at higher values of β. For example, in reference 12, the mean sonic line for an underexpanded convergent-divergent nozzle at $\beta = 2$ was still increasing in the radial direction at 10 diameters from the nozzle exit.

The mixing responsible for the reduction of shocks along the jet centerline at intermediate values of β is apparently enhanced by jet screech. Glass (ref. 13) has found that as jet stagnation pressure is increased, the plume pitot pressure at various measurement points along the jet axis exhibits discrete jumps. Sherman et al. (ref. 14) discovered that these jumps correspond to changes in the screech mode of the jet. Norum (ref. 2) found that the screech mode can change without a change in operating condition and that the downstream shock cell system changes at the instant of screech mode change. This phenomenon was quantitatively confirmed during the current test, as depicted in figure 10. Plotted here are the measured pitot pressures for three axial traverses performed at the same operating conditions ($\beta = 1.20$ and $U_f = 170$ fps). The measured pressure jumped from one mode to another and then back again during each of the three traverses. Although the presence of the probe in the flow may have somewhat influenced mode selection, the changes occurred at different axial locations for each traverse. Hence, considering the stringent tolerance maintained on the jet stagnation pressure during data acquisition, these apparently random mode changes must be caused by perturbations in the flow that are uncontrolled by standard laboratory methods. This behavior was found to exist for β between 1.0 and 1.2, with or without external flow.

In addition to mode switching with time at a given operating condition, changing the flight velocity also caused differences in mode selection. An example is illustrated in figure 11, which presents centerline static pressures from traverses at $\beta = 1.34$ at the static and flight conditions. Although both profiles are smooth, indicating a single mode existing throughout each traverse, it is apparent from differences in the number of shock cells and in the strengths of the downstream cells that different modes exist for the two traverses. As will be seen, the acoustic results are affected similarly by the external flow.

The appropriate length for scaling shock-associated noise is related to the shock cell spacing. This length can only be estimated, since cell spacing depends on cell number and since the downstream cell spacing can vary because of mode changes. In addition, the desire to choose a length that varies continuously with β conflicts with the desire to include the effect of the downstream cells. Because at least seven shock cells could be identified for each test condition, those conflicting desires were found to be best satisfied by choosing the average length of the

first seven cells, $\bar{L}_7$, as the representative length scale. Essentially identical values of $\bar{L}_7$ were computed from axial static pressure traverses at the centerline and near the lip line. Computations from centerline traverses at both the static and the flight condition are given in figure 12. Also shown is a straight line fit to the static data that will be used to scale the acoustic data. Note that there is a discernible increase in $\bar{L}_7$ at the flight condition for $\beta \geq 1.1$. This increase is mainly due to axial stretching of the jet by the external flow, although mode differences, as depicted in figure 11, may also have an influence.

ACOUSTIC RESULTS

The essential features of the differences in noise generation due to simulated flight with no mode changes can be seen in figure 13. Shown here are the far-field spectra for $\beta = 0.95$ measured at angles from 40° to 150° relative to the upstream axis. At each angle, the static and flight spectra (solid and dashed curves, respectively) are superimposed, with the ordinates for each angle displaced vertically for clarity. Each spectrum is a composite of screech, broadband shock-associated noise, and jet mixing noise. The screech component of shock-associated noise can be seen as a stationary tone and its higher harmonics. The effect of flight is to reduce the frequency of these tones and to change the directivity of at least the fundamental. The broadband shock noise dominates most of the spectra beyond the frequency of the fundamental screech tone, particularly at small angles to the upstream axis. The peak frequency of this broadband noise increases with angle because of an apparent Doppler effect. The strength of the screech makes this peak frequency difficult to pinpoint, although one can discern that it is shifted to a slightly lower frequency with simulated flight. The jet mixing noise can be seen in those parts of the spectra where shock-associated noise is absent or negligible, namely at the lower frequencies for all angles and at most frequencies for 150°. Flight reduces the mixing noise uniformly throughout the spectrum. The remainder of this section details the flight effects on each of the three components of supersonic jet noise.

Jet Mixing Noise

According to the commonly accepted method for computing the effects of flight on jet mixing noise (ref. 15), the ratio of the static value of mean square acoustic pressure to its flight value can be expressed as

$$\frac{\langle p^2 \rangle_{static}}{\langle p^2 \rangle_{flight}} = (1 - M_f \cos \phi)\left(\frac{U_j}{U_j - U_f}\right)^{m(\phi)} \tag{1}$$

where $m(\phi)$ is an empirically derived directivity exponent. Although this method was developed for shock-free jets, its applicability to the shock-containing underexpanded jets of the current investigation can be inferred from figure 14. Shown here is the difference between overall sound pressure levels (ΔOASPL) for static and flight conditions at the same nozzle pressure ratio, normalized by equation (1). The OASPL's were computed from the smoothed (screech tones removed) spectra measured at 150°. Results include 5 simulated flight speeds from 0 to 170 fps at 16 nozzle pressure ratios ranging from the sonic condition ($\beta = 0$) to $\beta = 1.8$. The value of OASPL at $U_f = 0$ was computed as the average of repeat runs at the given value of β. All the available data are shown in figure 14, and since repeat runs are

included, the spread at $U_f = 0$ is indicative of the repeatability of the computed OASPL. The data follow the indicated correlation quite well. The least squares straight line fit gives a slope (m) of 7.8, which falls within the range of exponents recommended as the standard for shock-free jets (ref. 15). (Shear layer angle corrections that would increase the computed slope only slightly were not included.) Hence, the mixing noise (OASPL) of shock-containing jets and shock-free jets decreases in flight according to the same relationship. This should be expected since it has been shown (ref. 11) that the development of the average turbulence and the spectra of the far-field jet mixing noise are the same for an underexpanded jet and a fully expanded jet operating at the same value of β.

Screech

The frequency of the dominant screech tone in an imperfectly expanded jet exhibits discrete jumps as the jet stagnation pressure is increased. Each jump in the frequency of the fundamental tone corresponds to a shift to a different screech mode. Five modes have been found by different investigators and were labeled in reference 16 as modes A_1, A_2, B, C, and D.

The behavior of the different screech modes of the test nozzle was determined by increasing the jet stagnation pressure in small increments and measuring the spectrum from the 40° microphone (with no external flow). The wavelength of the fundamental of each mode is presented in figure 15 along with the range of measurements (the shaded regions) of four previous investigators, taken from figure 2 of reference 2. The amplitude variation at the fundamental frequency at 40° from the upstream axis is given in figure 16. This figure shows that the most intense screech occurs between $\beta = 0.7$ and 1.3 and that the B and C modes attain about equal amplitudes. Recall from figure 7 that within this range of β, fewer shocks were found along the jet axis. This again implies that intense screech increases the jet mixing.

The expected change in the frequency of screech due to simulated flight can be estimated by considering the mechanism of screech generation. This process involves a feedback loop consisting of flow disturbances created at the nozzle lip, an oscillating shock structure, and upstream-traveling sound waves. The loop is maintained when the sound waves created at the oscillating shocks reinforce one another in the upstream direction, so that the sound impinging on the nozzle lip is intense enough to organize the flow disturbances. For maximum reinforcement to occur, the period of the fundamental screech frequency is equal to the sum of the travel times between successive shock cells of the downstream-traveling disturbance and the upstream-traveling sound wave. Hence,

$$T = \frac{L}{U_c} + \frac{L}{c_a - U_f} \tag{2}$$

where T is the period, L is the shock cell length, U_c is the disturbance convection velocity, and $c_a - U_f$ is the resultant speed of the sound waves

traveling against the external flow. Since the radiated wavelength λ of the screech tone is $c_a T$,

$$\frac{\lambda}{L} = \frac{1}{M_c} + \frac{1}{1 - M_f} \tag{3}$$

where M_c is the convection Mach number, U_c/c_a, and M_f is the Mach number of the external flow. The change in the average flow-disturbance convection velocity due to external flow is depicted in figure 17. The convection Mach number thus becomes

$$M_c = \frac{\alpha U_j}{c_a} + (1 - \alpha)M_f \tag{4}$$

where U_j is the fully expanded jet velocity and α has been empirically determined to be approximately 0.7 (refs. 3 and 17).

The extent to which equation (3) predicts the correct fundamental screech frequency is seen in figure 18. The value chosen for shock cell length in the experimental data was $\bar{L}_7$ as given in figure 12. The C mode is predicted quite well, although the screech wavelengths of the other modes are longer than those estimated from equation (3). This may be due to a lag that might exist between arrival of the flow disturbance and emission of the sound wave and vice versa, resulting in interaction times that have not been included in equation (2). Also, indications shown in figure 11 that the downstream shock cell development is remarkably different when the screech mode switches suggest that the shock cell length $\bar{L}_7$ used to compute λ/L for the experimental data may not be the correct length scale.

Nevertheless, an analytical estimate of the extent of the frequency shift of the fundamental screech tone with external flow can be obtained. The screech wavelengths at the flight and static conditions, λ_f and λ_o, respectively, were determined from equation (3). By assuming no change in the shock cell length with flight, the ratio of the two lengths was computed and plotted as the solid line in figure 19. In flight, the decrease in disturbance travel time due to the increasing convection velocity is more than compensated by the increase in travel time of the upstream-traveling sound wave; thus, the screech wavelength increases. The ratios of measured wavelengths are given by the symbols in figure 19. Outside the region between $\beta = 1.1$ and 1.4, the prediction based on equation (3) is remarkably good. The increase in the prediction with flight due to neglect of interaction time is apparently offset by the neglect of slightly longer shock cell lengths.

The disagreement in the intermediate range of β in figure 19 is due to mode changes. This can be seen in figure 20, which gives the measured wavelength of the fundamental of the dominant screech mode. At the flight condition, a dominant C mode does not exist at any value of β. The switch from the C mode at a given value of β was found to occur at a forward speed that varied with β. Figure 20 also suggests, from the continuous wavelength variation for the flight condition, that there may actually be little difference between the B and D screech modes.

Static pressure profiles at a condition for which a mode change occurs because of changing flight speed were given in figure 11. These profiles show that the number of shock cells is smaller and hence the jet mixing greater for the flight condi-

tion, which corresponds to the B or D screech mode. A similar result was obtained by shadowgraph visualization in reference 2, where the number of shock cells was found to decrease when the C screech mode was changed to the B mode by the use of a reflecting baffle.

To estimate the screech wavelength difference due to changing shock cell spacings caused by mode change, the average cell length over the entire shock cell system was computed for $\beta = 1.34$ from figure 11. For the static condition, the 11 shock cells have an average length of 1.45d, whereas the 8 discernible shock cells for the flight condition yield an average length of 1.65d. If the ratio of these two lengths is used to modify the theoretical wavelength ratio, given as 1.06 at $\beta = 1.34$ in figure 19, we obtain a corrected value of 1.21, which is remarkably close to the measured wavelength ratio shown in figure 19. Hence the differences between theoretical and predicted screech wavelengths may be entirely attributable to an incorrect choice for the appropriate shock length scale.

Broadband Shock Noise

Since the strength of the screech process makes it difficult to determine the amplitude of the broadband component of shock noise, no attempt was made to estimate the effect of flight on this amplitude. However, since the broadband spectrum changes with observer angle, it is relatively easy to determine the peak frequency. It was found that the value estimated for the peak frequency from the 90° microphone spectrum agreed quite well with that interpolated from peak frequencies measured at other observer angles. This latter method for determining the peak frequency is described in detail in reference 17.

Before presenting the experimental results, an attempt is made to predict the effect of flight on the broadband noise peak frequency. According to the most widely accepted model for broadband shock-associated noise (ref. 3), phase differences between the noise generated at successive shocks account for its spectral characteristics. The peak frequency of the broadband shock noise has a period equal to the time required for a flow disturbance to travel one shock cell plus the difference between propagation times of the waves generated at successive shocks. Hence, as can be seen in figure 21, this period is

$$T = \frac{L}{U_c} + \frac{L \cos \psi}{c_a} \tag{5}$$

where ψ is the far-field observer angle. The wavelength of this broadband spectral peak is then

$$\frac{\lambda}{L} = \frac{1}{M_c} + \cos \psi \tag{6}$$

Since the actual microphones are at a finite distance from the nozzle, ψ is not the true far-field angle and equation (6) should be modified for geometrical effects. To simplify the analysis, the observer angle ψ can be limited to 90° as shown in figure 22. Letting the source distribution be centered at a distance x_s

from the center of the microphone arc, a better approximation for the broadband peak wavelength is

$$\frac{\lambda}{L} = \frac{1}{M_c} + \cos \phi \tag{7}$$

From the geometry of figure 22,

$$x_s = \frac{r_f}{\tan \theta} + \frac{r_m - r_f}{\tan \phi} \tag{8}$$

where r_f is the radius of the free jet and r_m is the radius of the microphone arc. The velocity triangle yields

$$c_a \sin(\theta - \phi) = U_f \sin(\pi - \theta) \tag{9}$$

which when combined with equation (8) gives

$$\cos \phi = \frac{M_f r_f r_m + x_s (r_m^2 + x_s^2 - M_f^2 r_f^2)^{1/2}}{r_m^2 + x_s^2} \tag{10}$$

The peak wavelength of the broadband noise at the 90° microphone without external flow is shown in figure 23 along with predictions from equations (6) and (7). The average cell lengths $\bar{L}_7$ were again used to nondimensionalize the measured results. The source location needed to compute $\cos \phi$ was chosen to be equal to the center of the measured shock cell distribution. A reasonably good comparison between predicted and measured wavelengths is obtained.

The ratios of the measured peak wavelengths at the flight condition to those measured statically are shown in figure 24 along with the ratios predicted from equations (6) and (7). The predicted ratios are less than unity, indicating smaller wavelengths (higher frequencies) in flight, which is opposite to what actually occurs. Corrections to the predictions for the increased shock spacings in flight, taken from figure 12, lead to somewhat better agreement, although the predicted wavelength ratios are still less than those measured.

Note that for β between 1.1 and 1.4, the measured broadband peak wavelengths are much higher than predicted, as was found for the screech wavelengths. This implies that the changing structure of the downstream shock cells that accompanies screech mode changes strongly influences the broadband noise radiation. Hence, in agreement with deductions based on near-field measurements (ref. 17), the downstream shock cells appear to be the most influential in determining the shock-associated noise.

CONCLUSIONS

Far-field acoustic pressure and mean plume static and pitot pressures were measured for an underexpanded jet with and without simulated flight. It was found that the effect of flight on jet mixing noise from shock-containing jets was virtually identical to its effect on mixing noise from shock-free jets. The frequencies of both components of shock-associated noise were found to decrease with forward speed. At conditions for which the screech mode did not change with flight, the screech wavelength change was predicted well by theory, whereas the wavelength change of the peak broadband shock noise was not. At all test nozzle pressure ratios, the jet centerline static pressures at flight speeds of 0 and 170 fps are virtually identical over the first seven or eight jet diameters; only if shocks exist further downstream is their spacing increased by the external flow.

Over a wide range of nozzle pressure ratios the dominant screech mode changed with an increase in flight speed. These mode changes were accompanied by large changes in both the downstream shock structure and the characteristics of the broadband shock-associated noise. The fact that the upstream shocks are virtually unchanged under these circumstances gives strong evidence that the characteristics of shock-associated noise are determined by the weaker downstream shock cells.

Langley Research Center
National Aeronautics and Space Administration
Hampton, VA 23665
April 16, 1984

REFERENCES

1. Powell, Alan: On the Noise Emanating From a Two-Dimensional Jet Above the Critical Pressure. Aeronaut. Q., vol. IV, pt. 2, Feb. 1953, pp. 103-122.

2. Norum, T. D.: Screech Suppression in Supersonic Jets. AIAA J., vol. 21, no. 2, Feb. 1983, pp. 235-240.

3. Harper-Bourne, M.; and Fisher, M. J.: The Noise From Shock Waves in Supersonic Jets. Noise Mechanisms, AGARD-CP-131, Mar. 1974, pp. 11-1 - 11-13.

4. Tanna, H. K.; Dean, P. D.; and Burrin, R. H.: The Generation and Radiation of Supersonic Jet Noise. Volume IV - Shock-Associated Noise Data. AFAPL-TR-76-65, Vol. IV, U.S. Air Force, Sept. 1976. (Available from DTIC as AD A032 883.)

5. Norum, Thomas D.; and Seiner, John M.: Measurements of Mean Static Pressure and Far-Field Acoustics of Shock-Containing Supersonic Jets. NASA TM-84521, 1982.

6. Hay, J. A.; and Rose, E. G.: In-Flight Shock Cell Noise. J. Sound & Vib., vol. 11, no. 4, Apr. 1970, pp. 411-420.

7. Drevet, P.; Duponchel, J. P.; and Jacques, J. R.: The Effect of Flight on Jet Noise as Observed on the Bertin Aerotrain. J. Sound & Vib., vol. 54, no. 2, Sept. 22, 1977, pp. 173-201. (Available as AIAA Paper No. 76-557.)

8. Bryce, W. D.; and Pinker, R. A.: The Noise From Unheated Supersonic Jets in Simulated Flight. AIAA Paper 77-1327, Oct. 1977.

9. Sarohia, V.: Some Flight Simulation Experiments on Jet Noise From Supersonic Underexpanded Flows. AIAA J., vol. 16, no. 7, July 1978, pp. 710-716.

10. Hubbard, Harvey H.; and Manning, James C.: Aeroacoustic Research Facilities at NASA Langley Research Center - Description and Operational Characteristics. NASA TM-84585, 1983.

11. Seiner, J. M.; and Norum, T. D.: Aerodynamic Aspects on Shock Containing Jet Plumes. AIAA Paper 80-0965, June 1980.

12. Seiner, John M.; and Norum, Thomas D.: Experiments on Shock Associated Noise of Supersonic Jets. AIAA Paper 79-1526, July 1979.

13. Glass, David R.: Effects of Acoustic Feedback on the Spread and Decay of Supersonic Jets. AIAA J., vol. 6, no. 10, Oct. 1968, pp. 1890-1897.

14. Sherman, P. M.; Glass, D. R.; and Duleep, K. G.: Jet Flow Field During Screech. Appl. Sci. Res., vol. 32, no. 3, Aug. 1976, pp. 283-303.

15. Gas Turbine Jet Exhaust Noise Prediction. ARP 876C, Soc. Automot. Eng., Inc., Sept. 1982. (Supersedes ARP 876B.)

16. Davies, M. G.; and Oldfield, D. E. S.: Tones From a Choked Axisymmetric Jet. Acustica, vol. 12, no. 4, 1962, pp. 257-277.

17. Norum, T. D.; and Seiner, J. M.: Broadband Shock Noise From Supersonic Jets. AIAA J., vol. 20, no. 1, Jan. 1982, pp. 68-73.

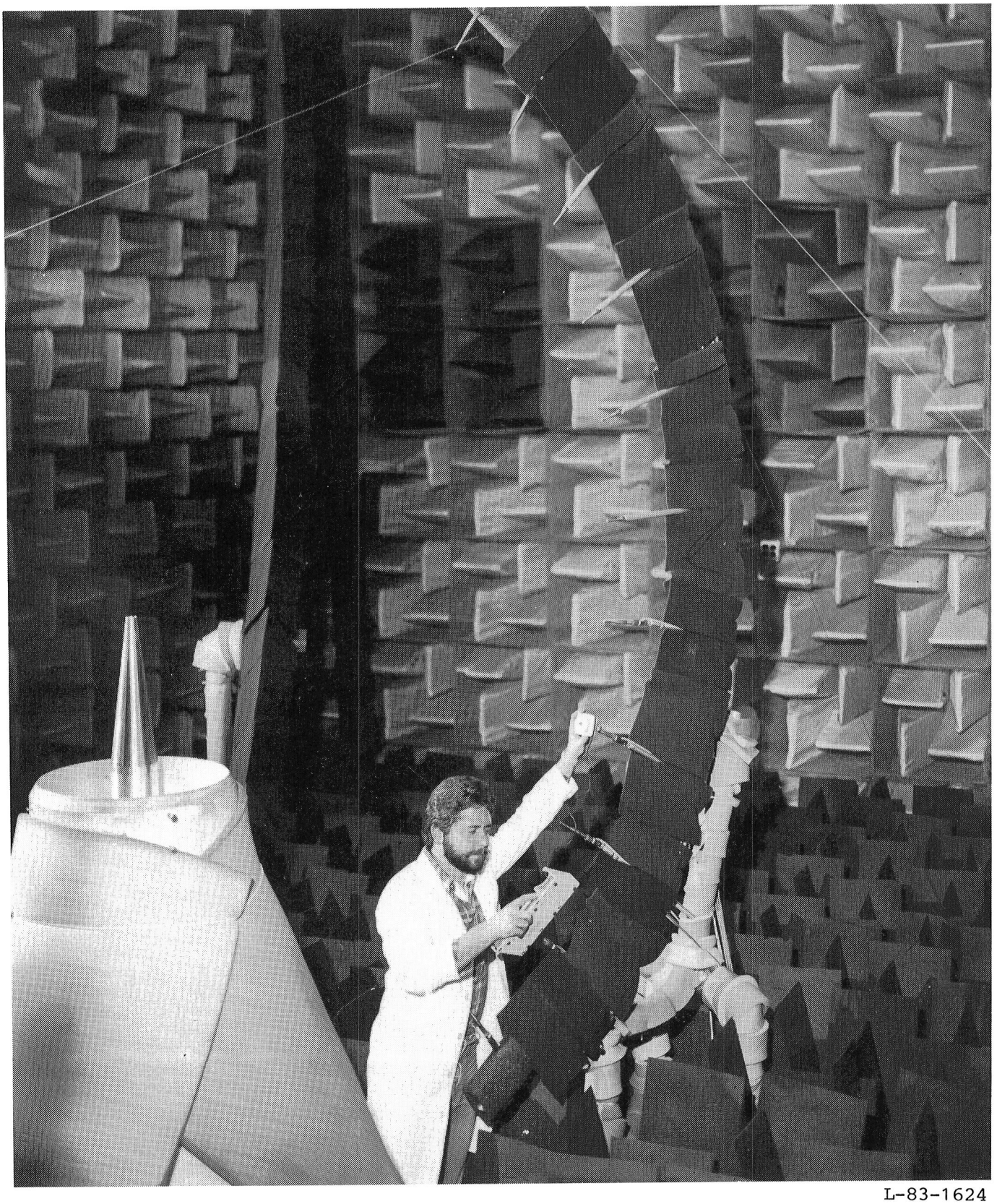

L-83-1624

Figure 1.- Nozzles and microphones mounted in anechoic chamber.

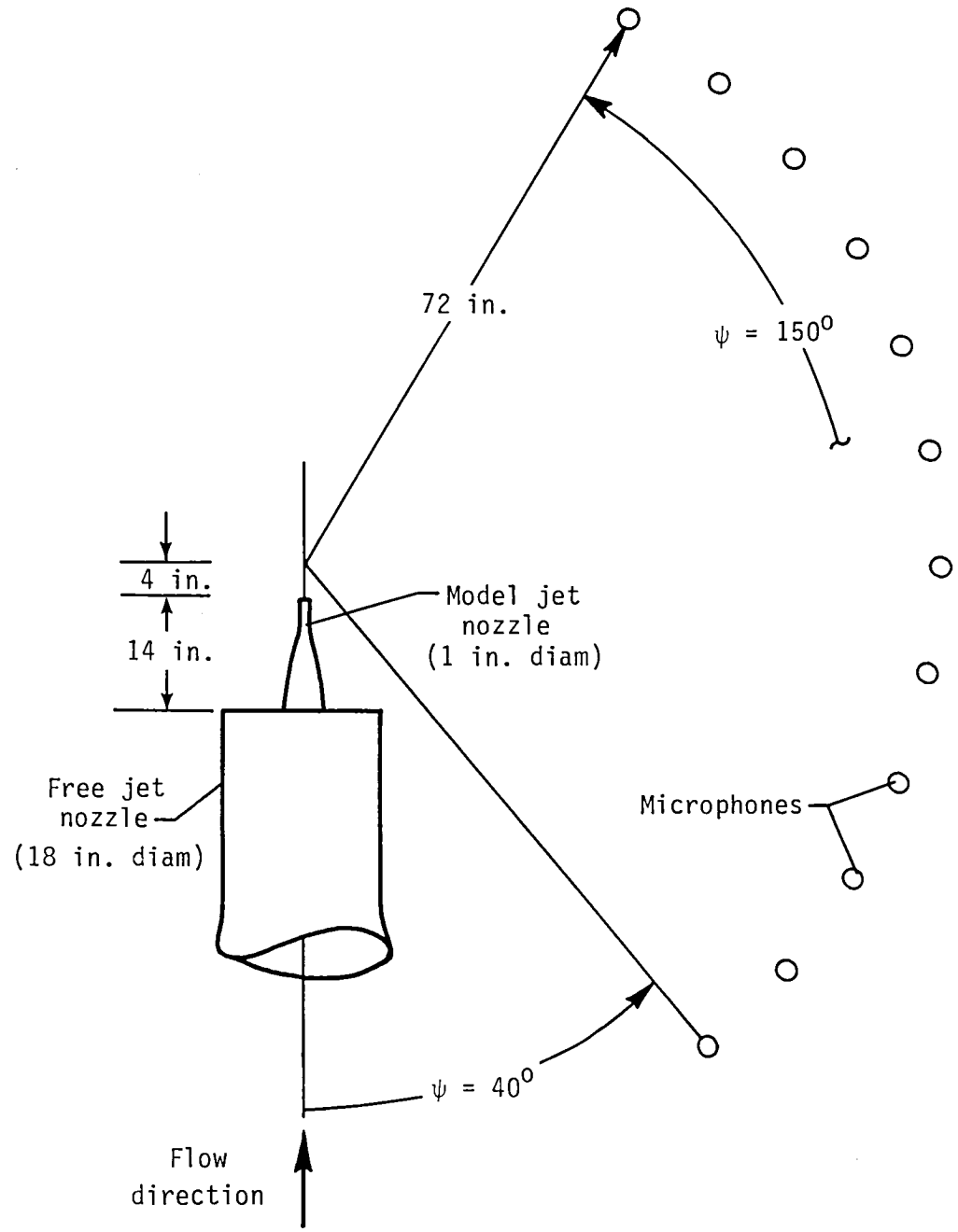

Figure 2.- Sketch of experimental arrangement for acoustic tests.

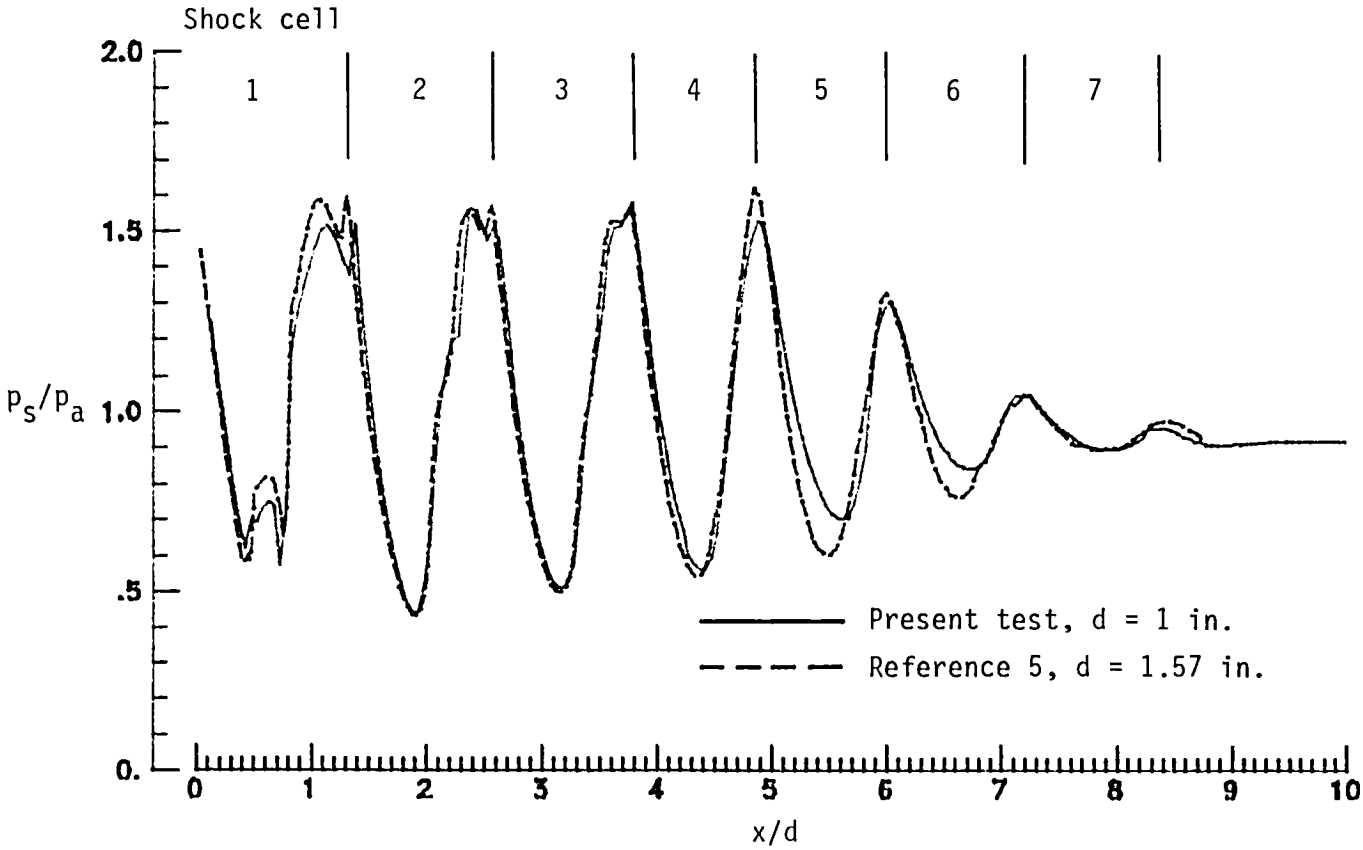

Figure 3.- Centerline static pressure distribution at $\beta = 1.0$ and $U_f = 0$.

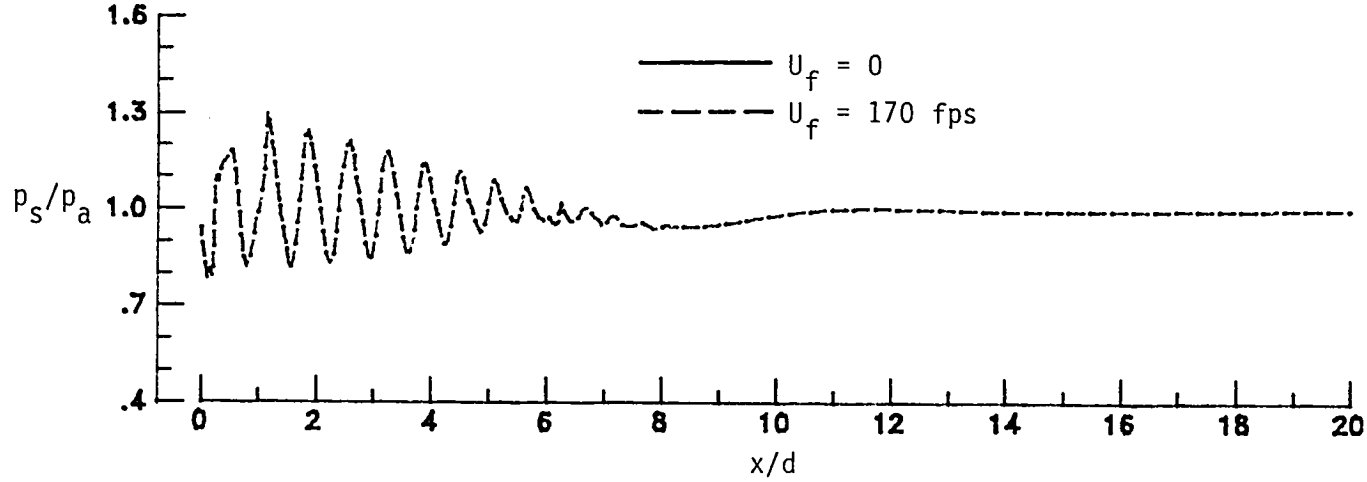

(a) $\beta = 0.60$

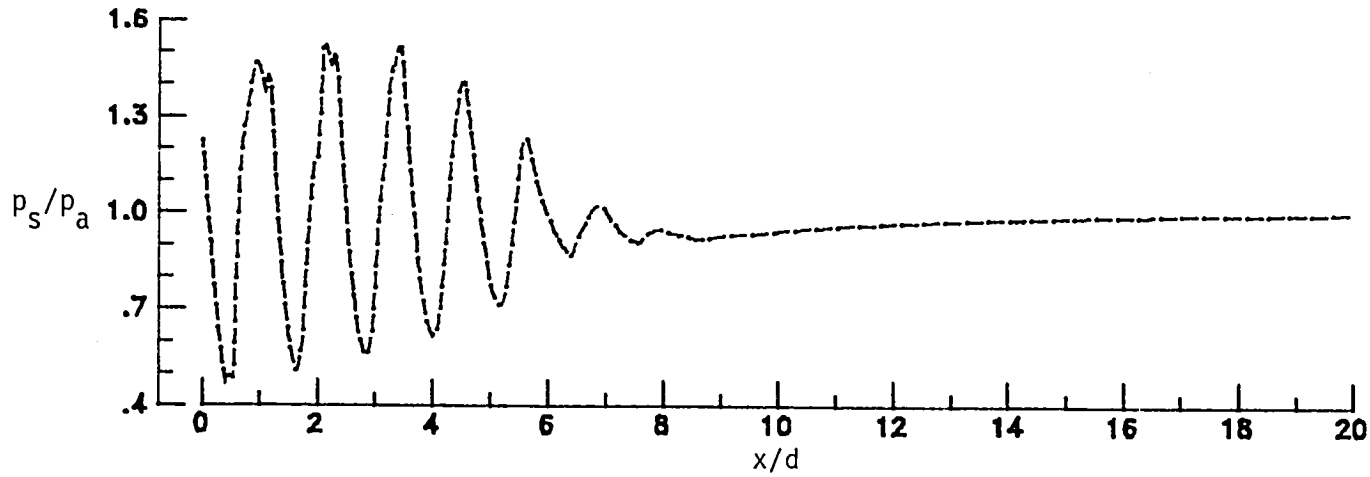

(b) $\beta = 0.94$.

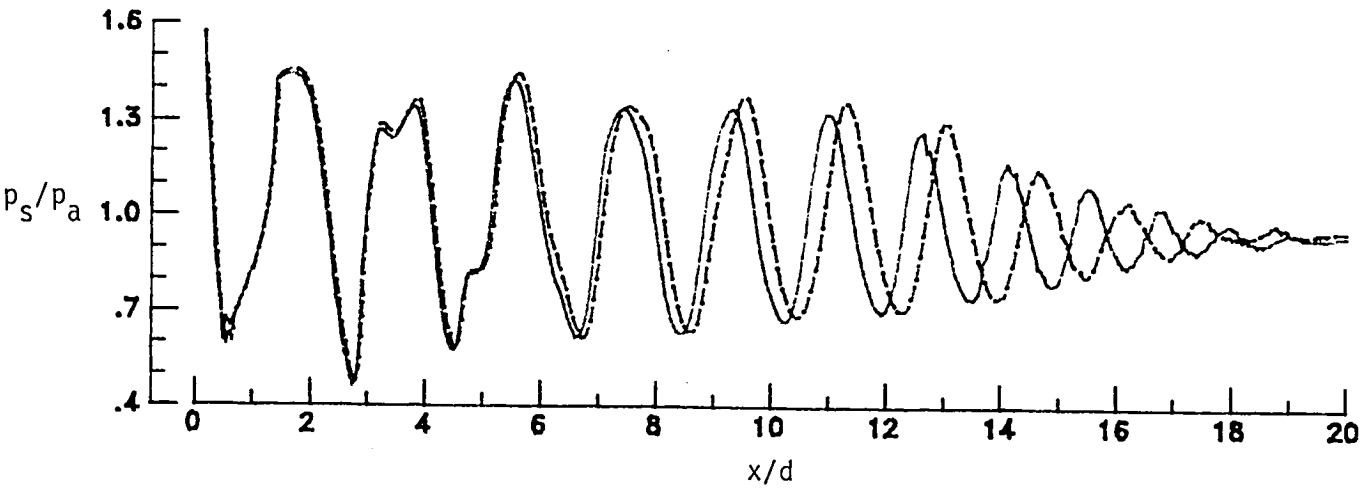

(c) $\beta = 1.50$.

Figure 4.- Centerline static pressure distributions.

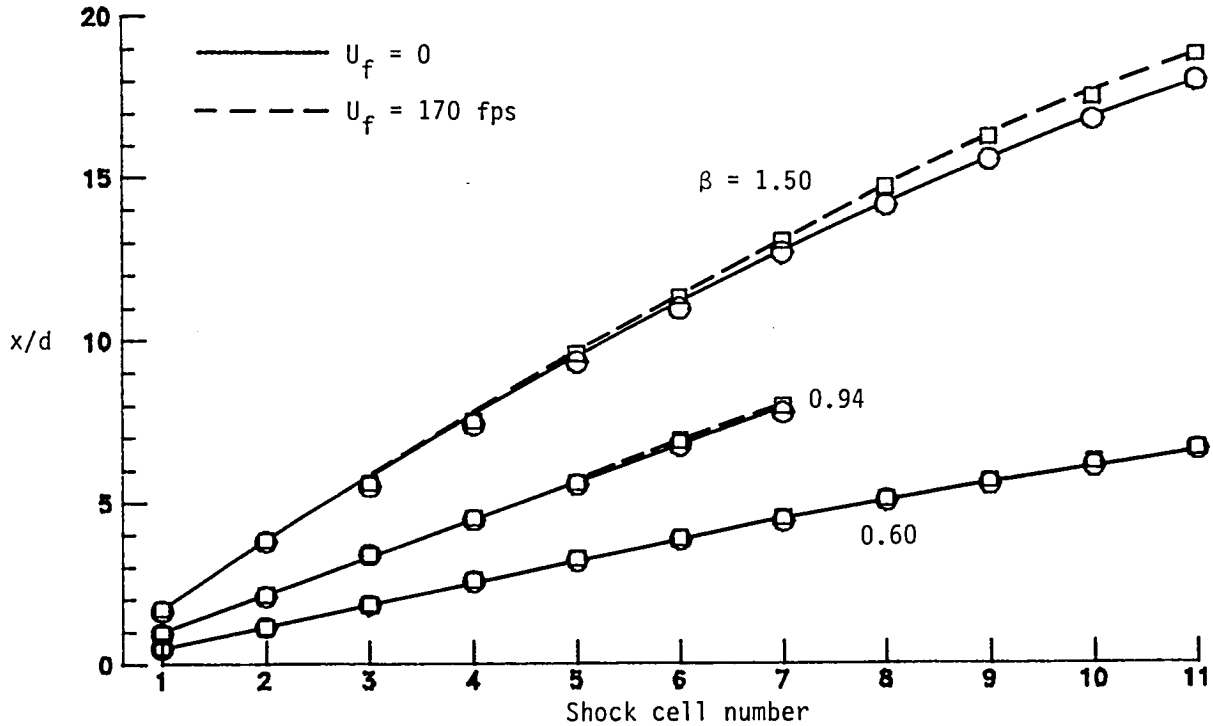

Figure 5.- Axial location of shocks along jet centerline.

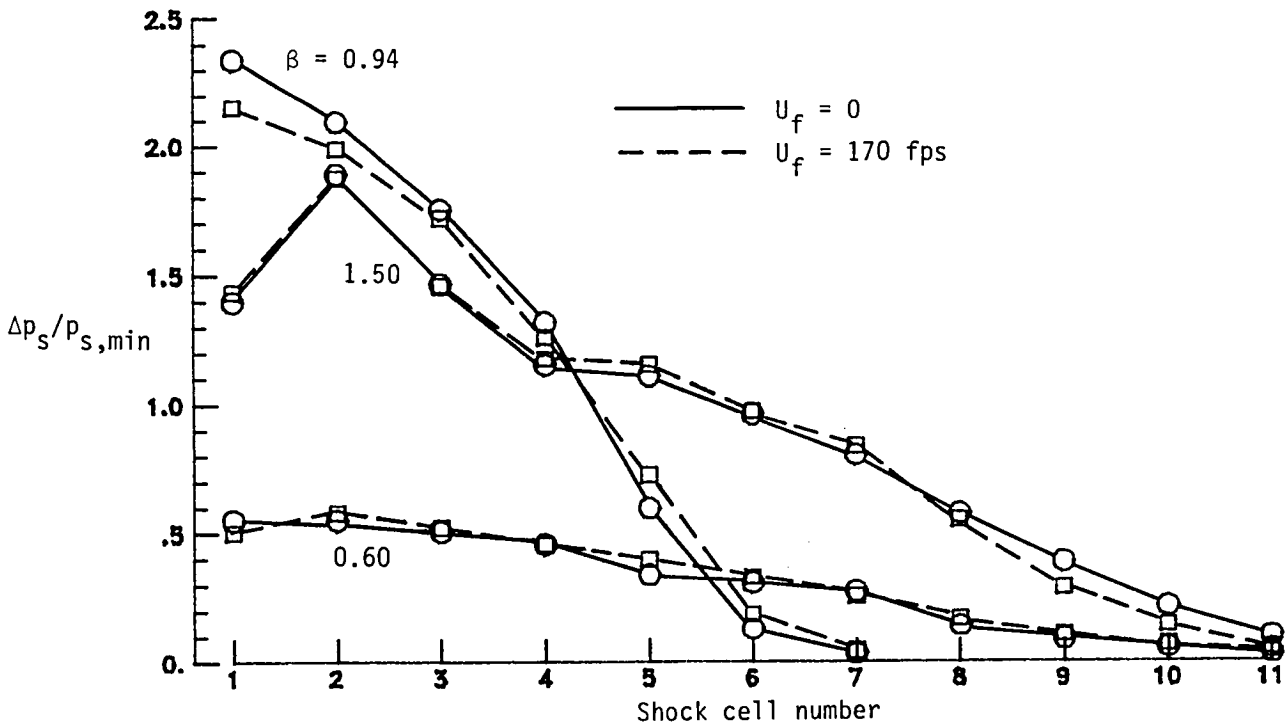

Figure 6.- Shock cell strengths measured along jet centerline.

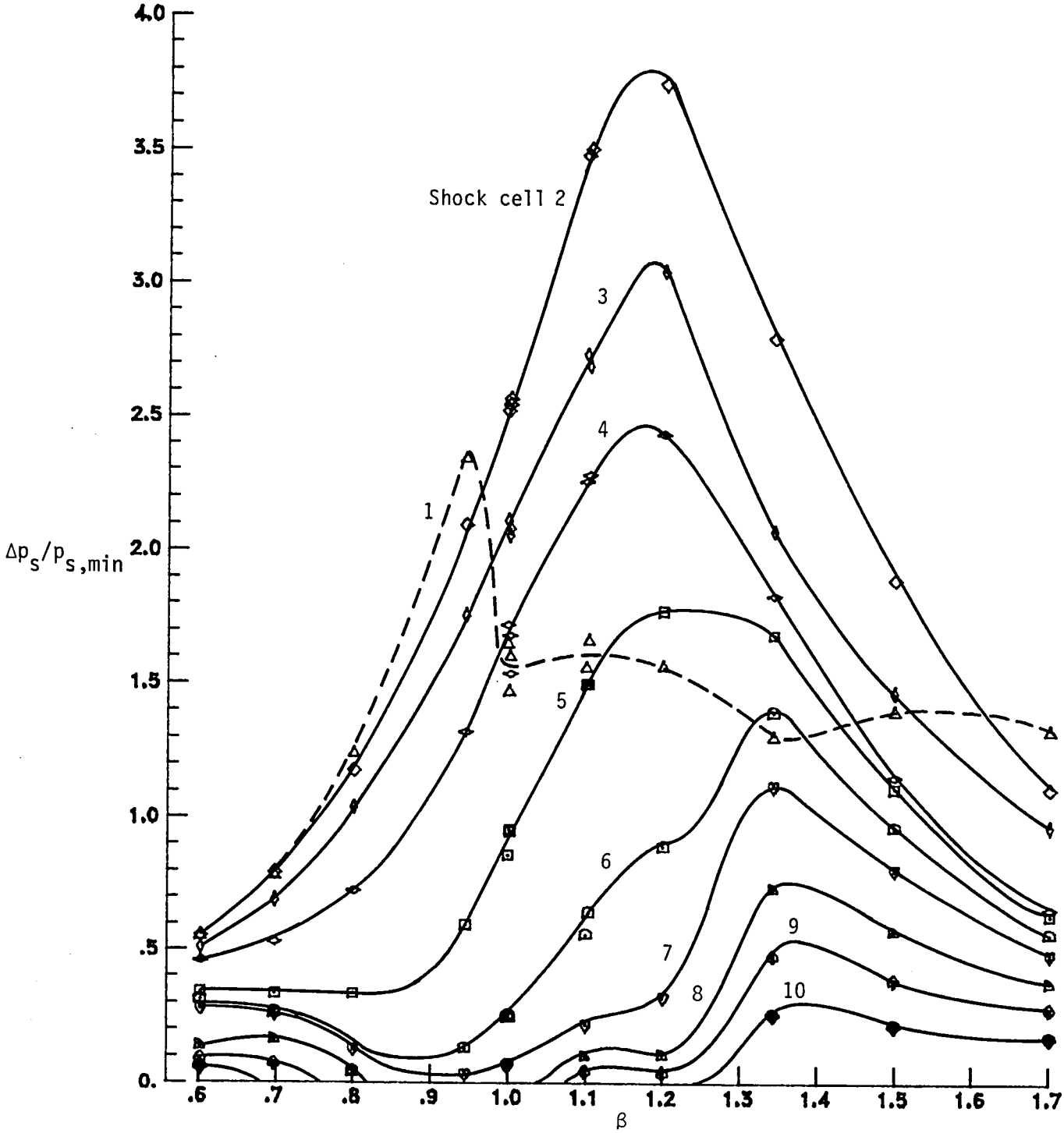

Figure 7.- Shock cell strengths at the static condition measured along jet centerline.

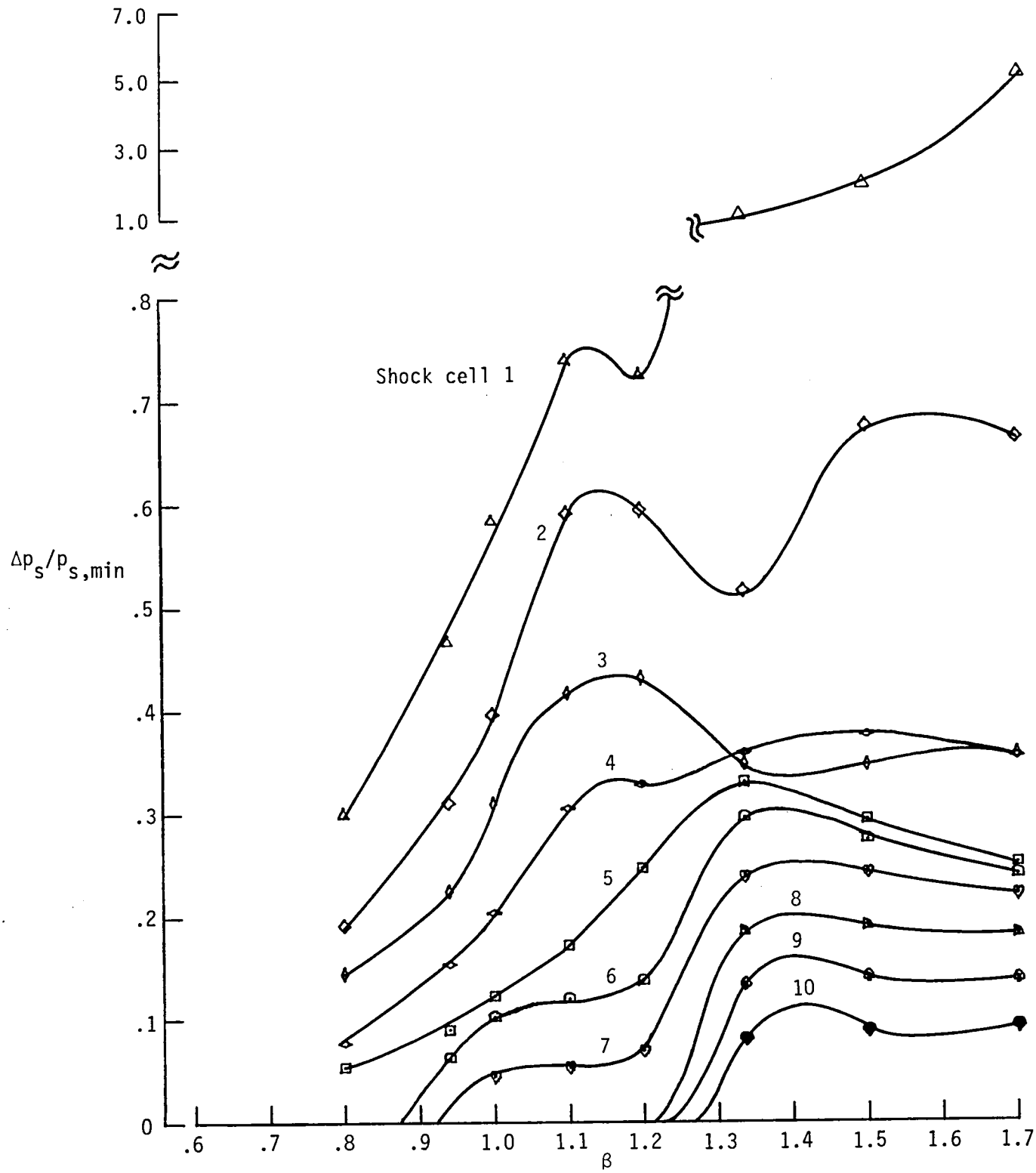

Figure 8.- Shock cell strengths at the static condition measured near nozzle lip line (r/d = 0.45).

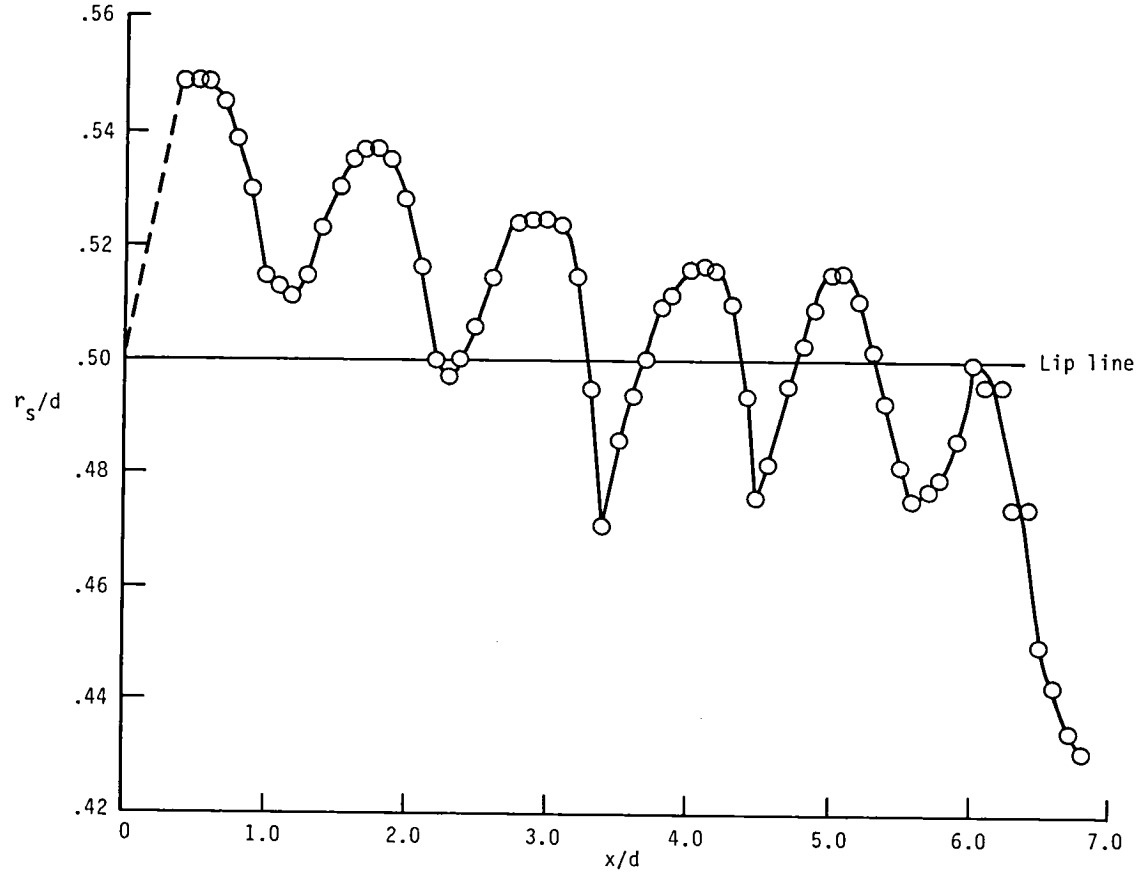

Figure 9.- Variation of the sonic line radius at $\beta = 0.94$ at the static condition.

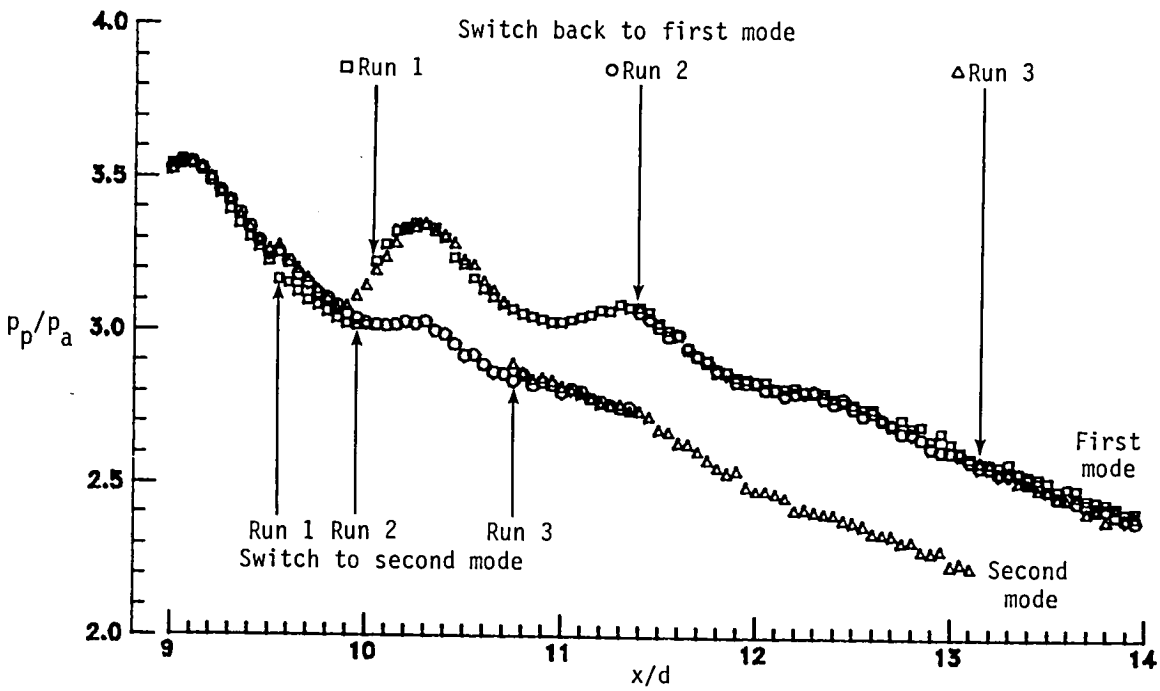

Figure 10.- Pitot pressure distributions from three independent traverses (runs 1, 2, and 3) along the jet centerline at $\beta = 1.20$ and $U_f = 170$ fps.

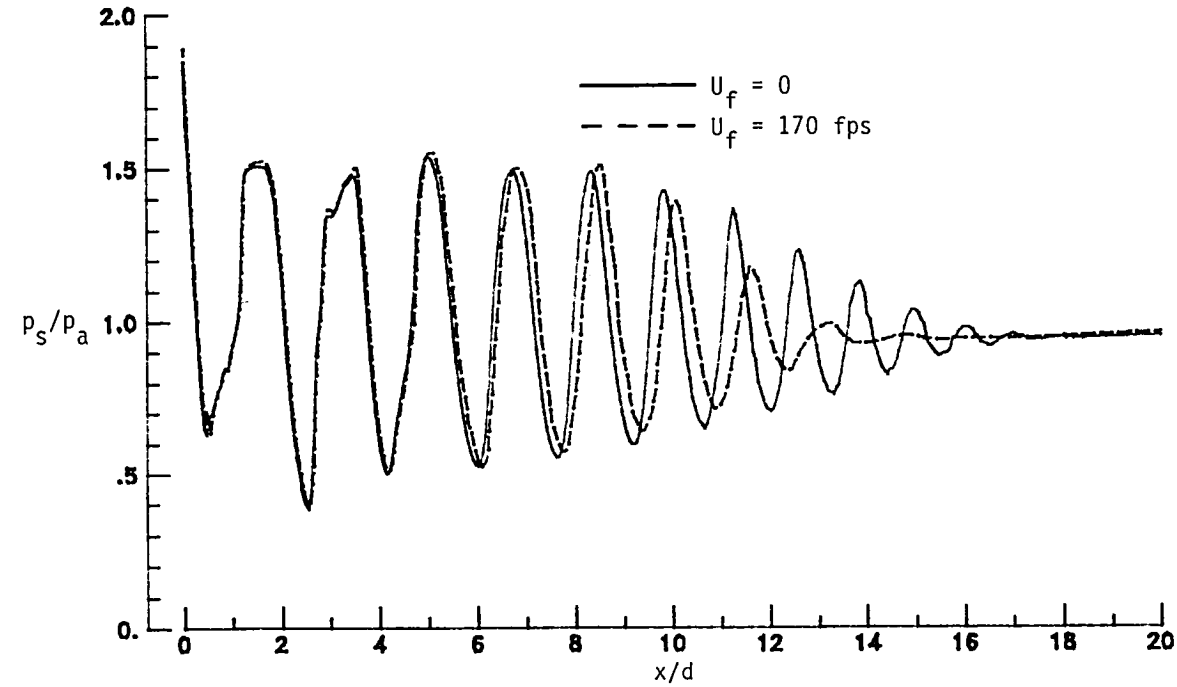

Figure 11.- Centerline static pressure distributions at $\beta = 1.34$.

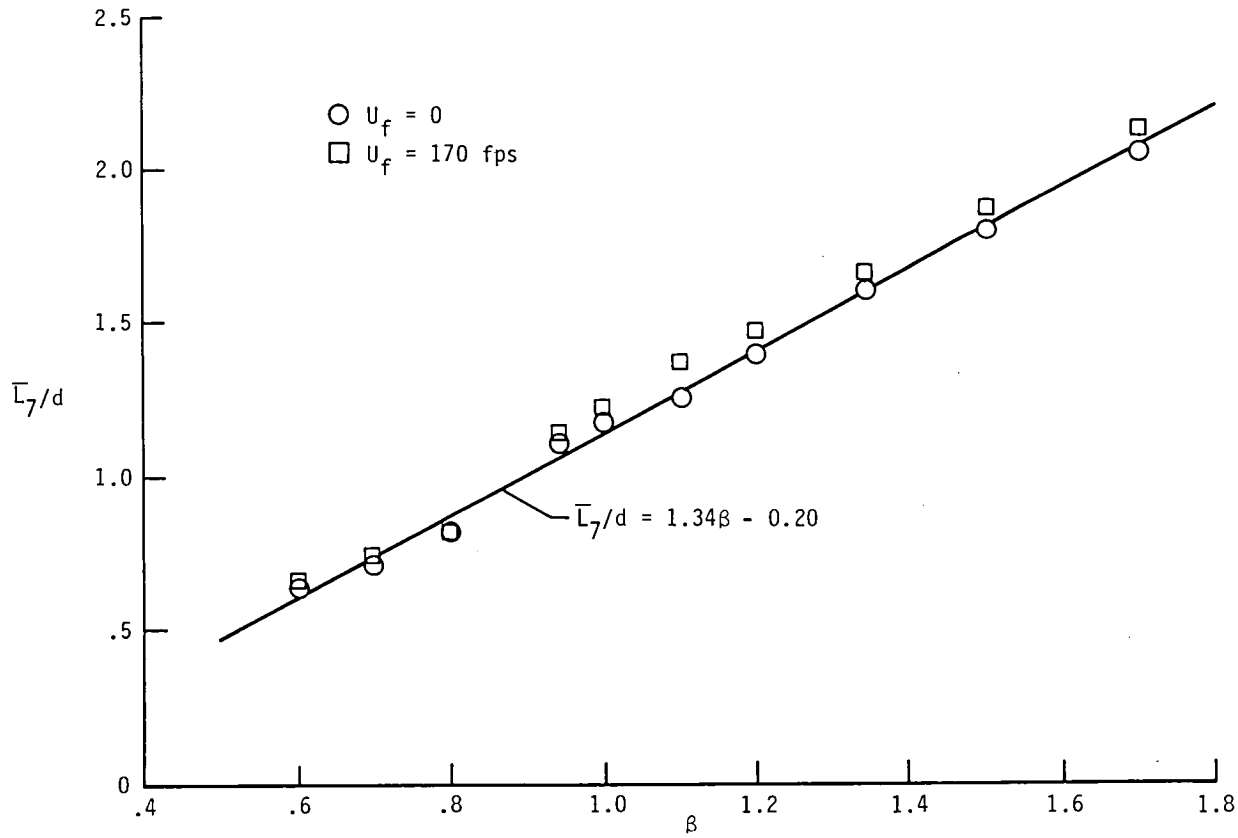

Figure 12.- Average spacing of first seven shock cells from centerline static pressure traverses.

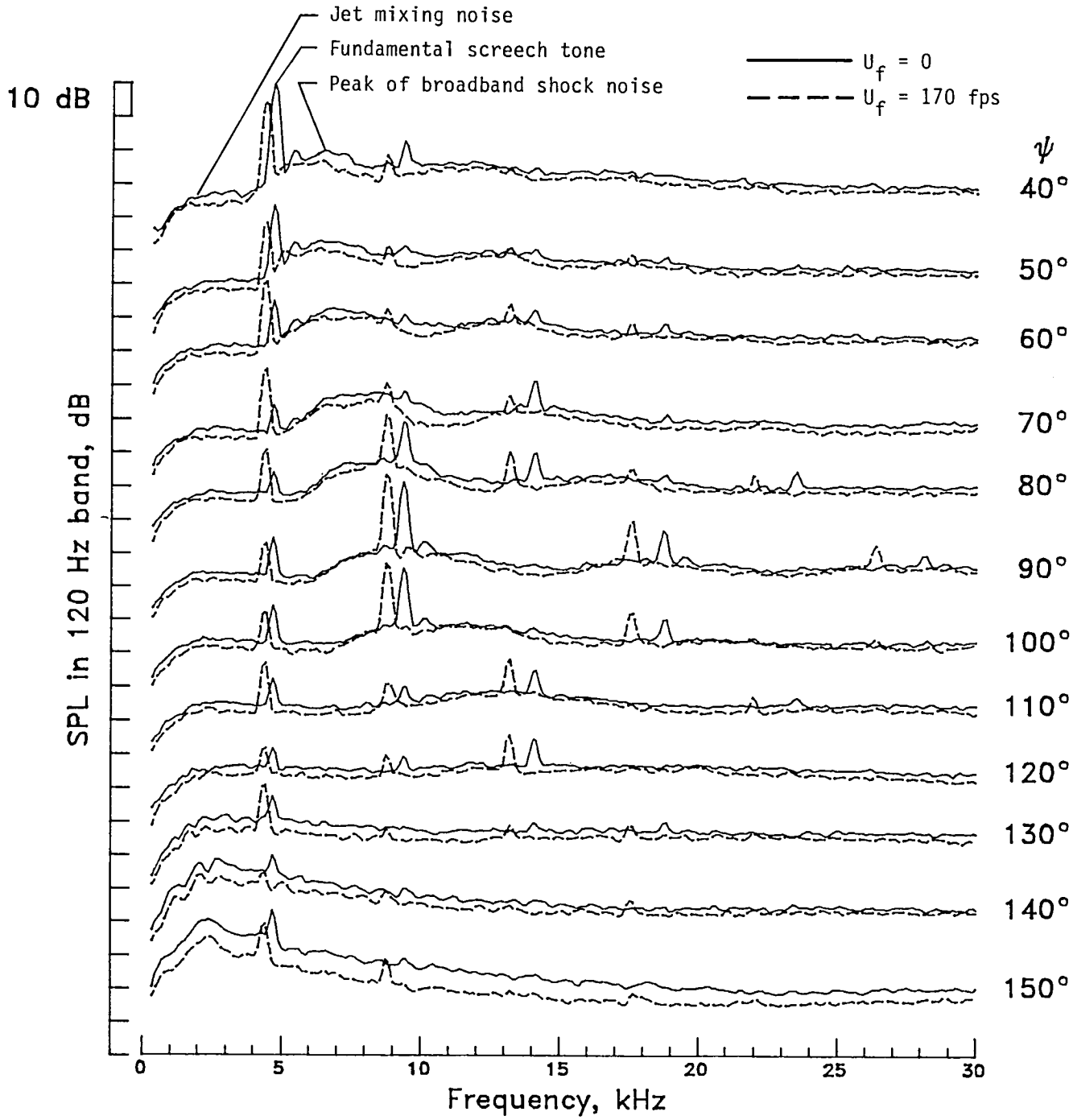

Figure 13.- Far-field noise spectra at $\beta = 0.95$.

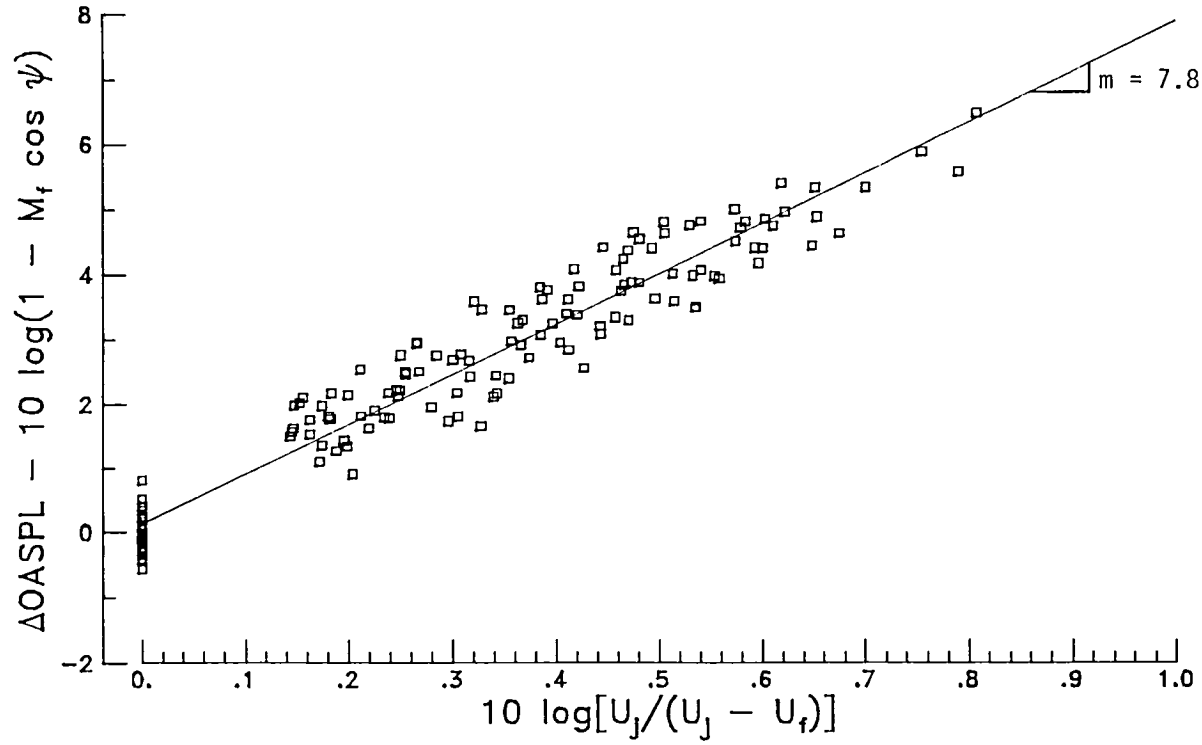

Figure 14.- Behavior of supersonic jet mixing noise with simulated forward motion.

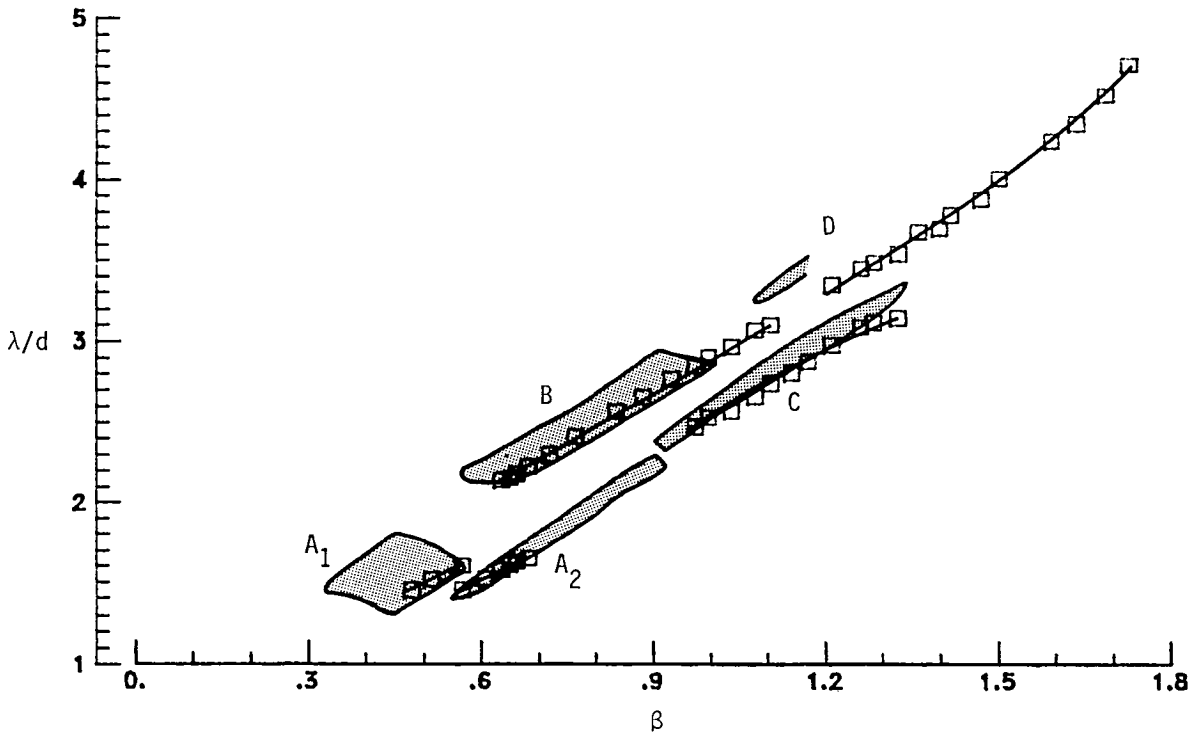

Figure 15.- Wavelengths of fundamental screech tones. Shaded areas represent data from previous investigations.

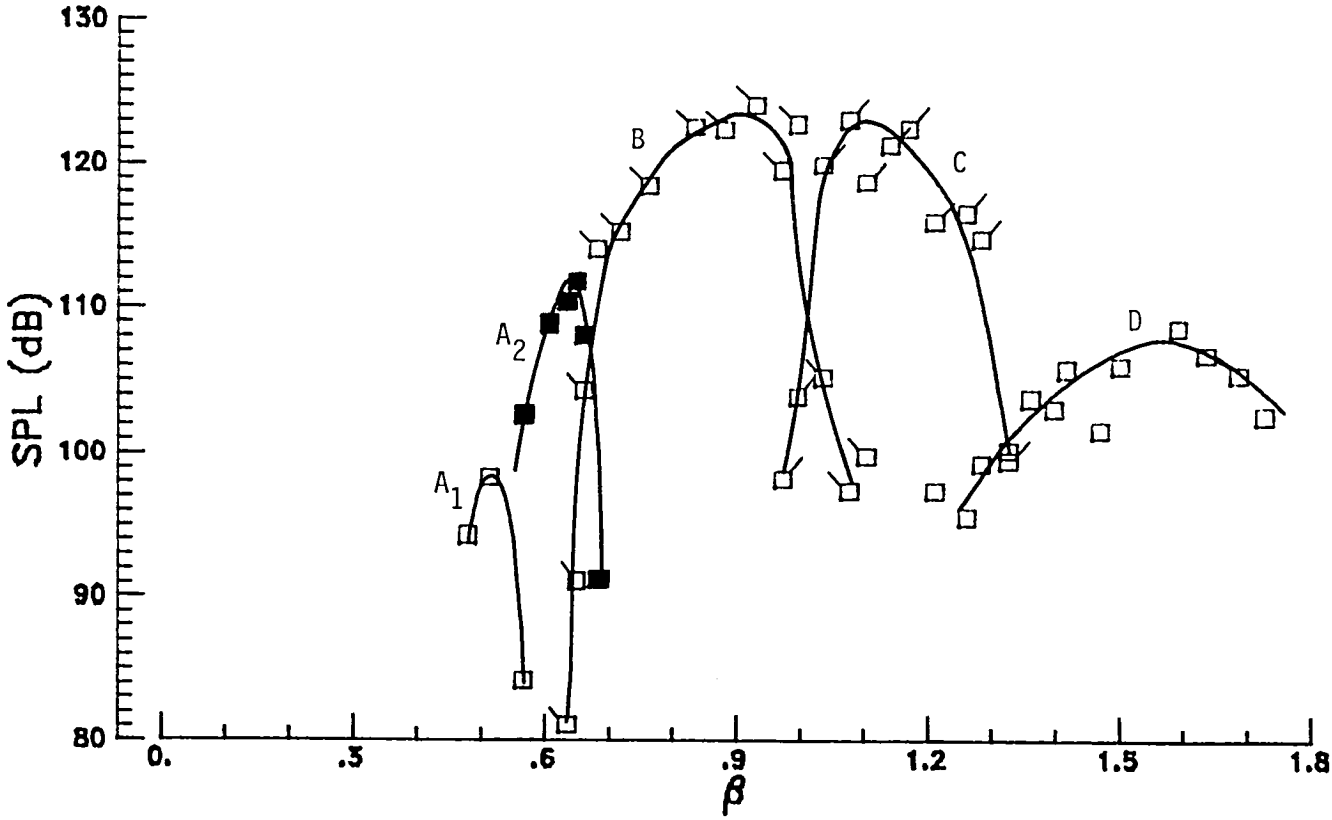

Figure 16.- Sound pressure levels of fundamental screech tones measured at 40° from the upstream axis.

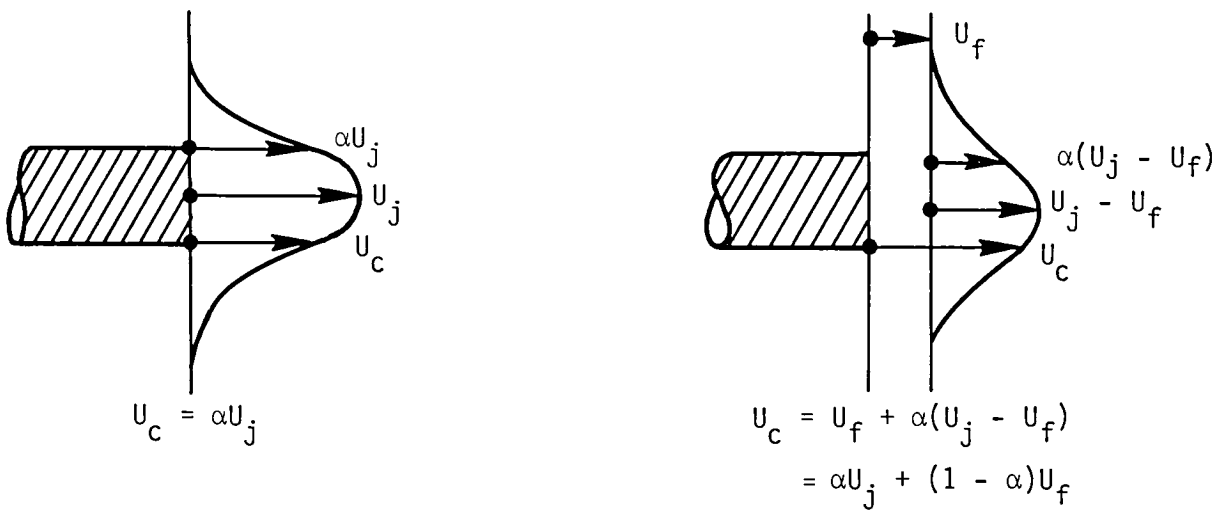

Figure 17.- Flow-disturbance convection velocity with and without external flow.

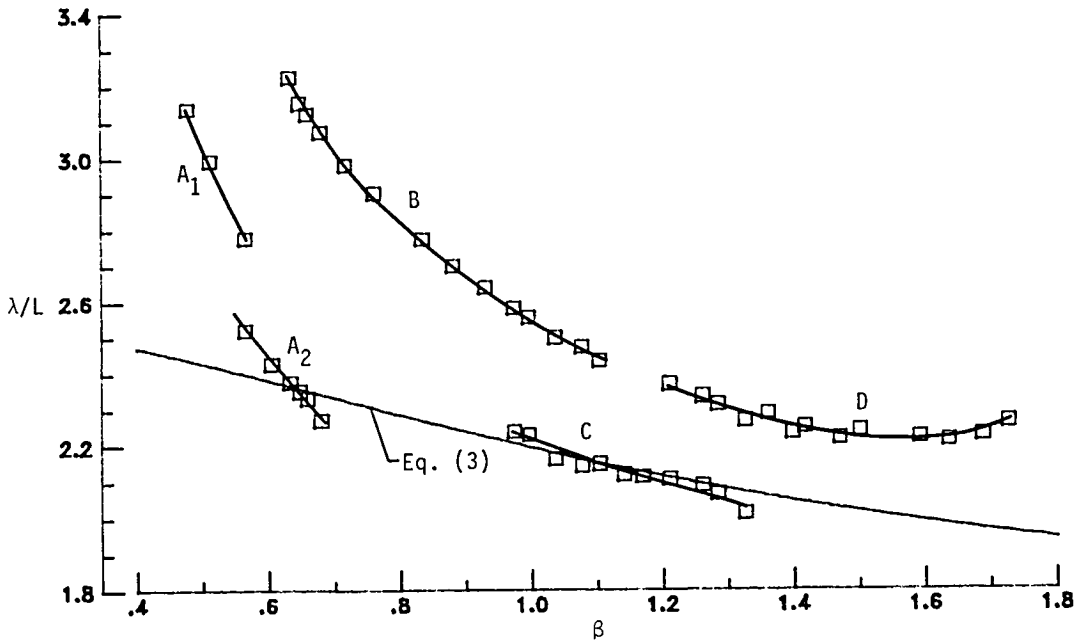

Figure 18.- Ratio of wavelength of fundamental screech tone to shock cell spacing.

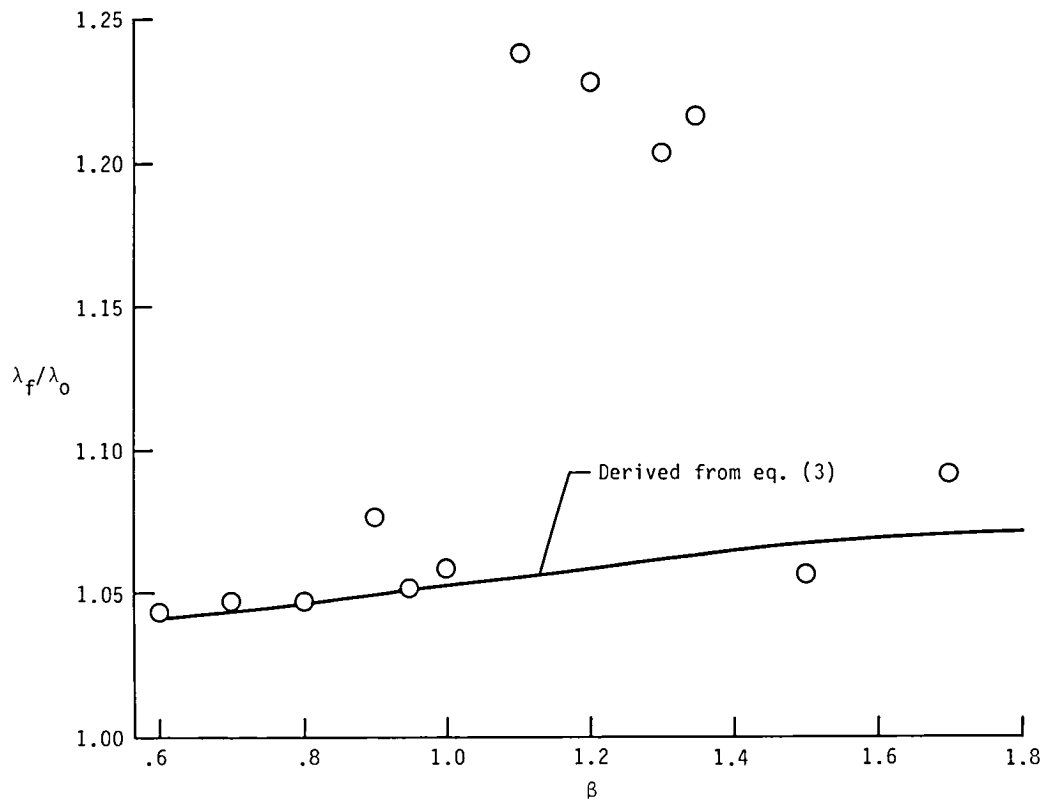

Figure 19.- Ratio of flight wavelength to static wavelength of fundamental tone of dominant screech mode.

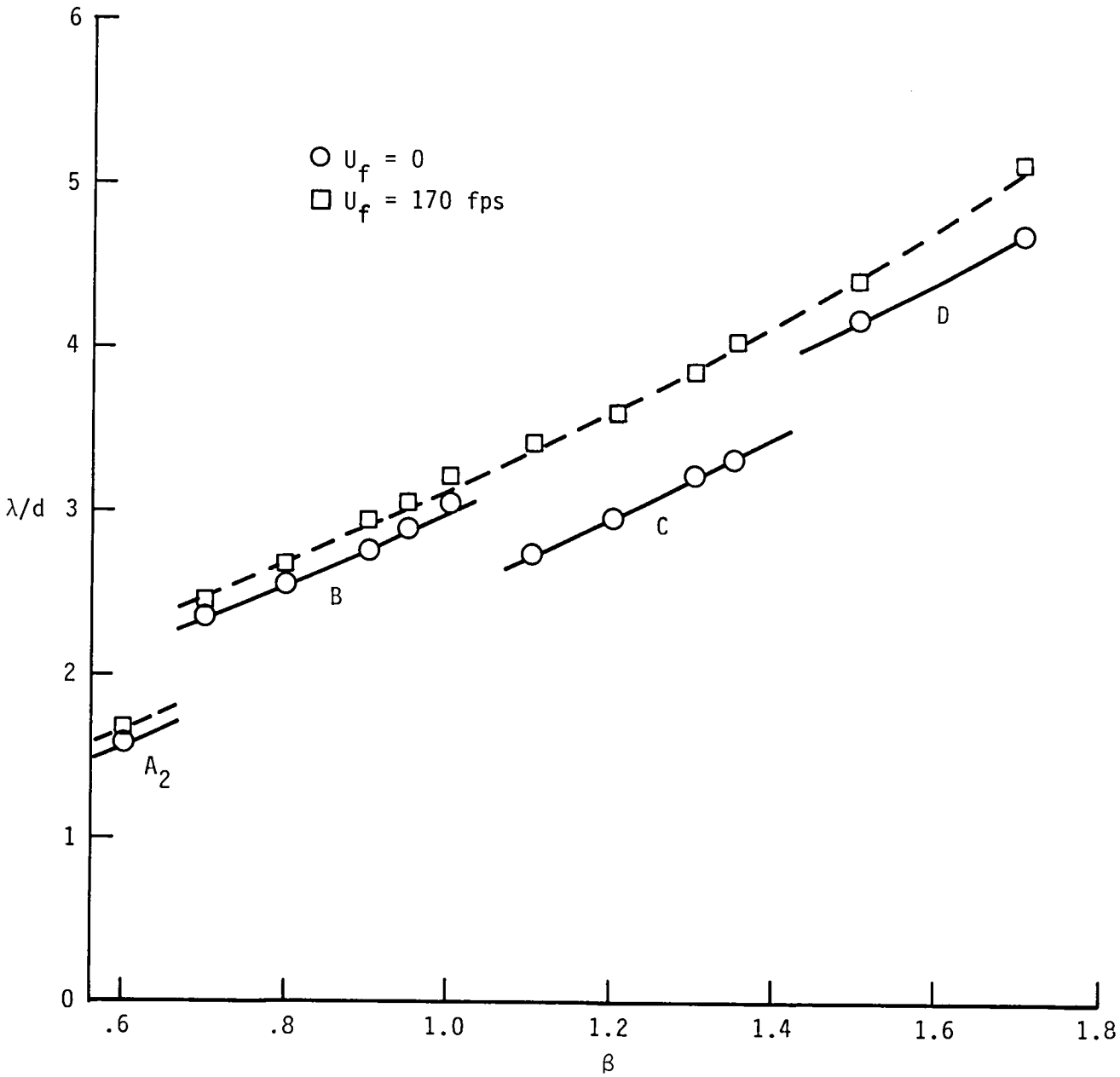

Figure 20.- Wavelengths of fundamental tones of dominant screech mode.

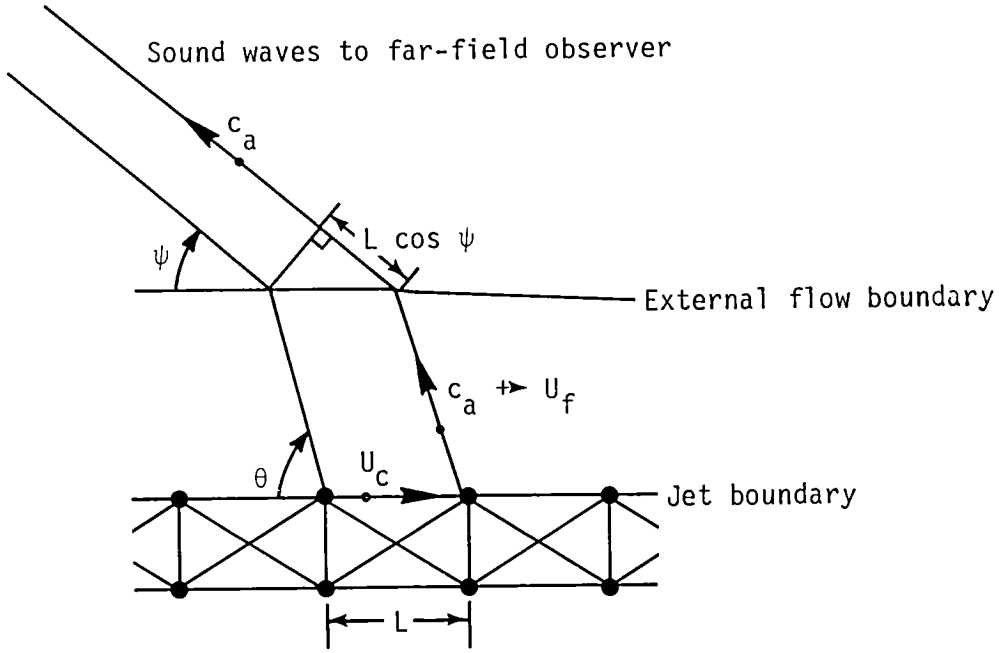

Figure 21.- Propagation of broadband shock noise to far-field observer angle ψ.

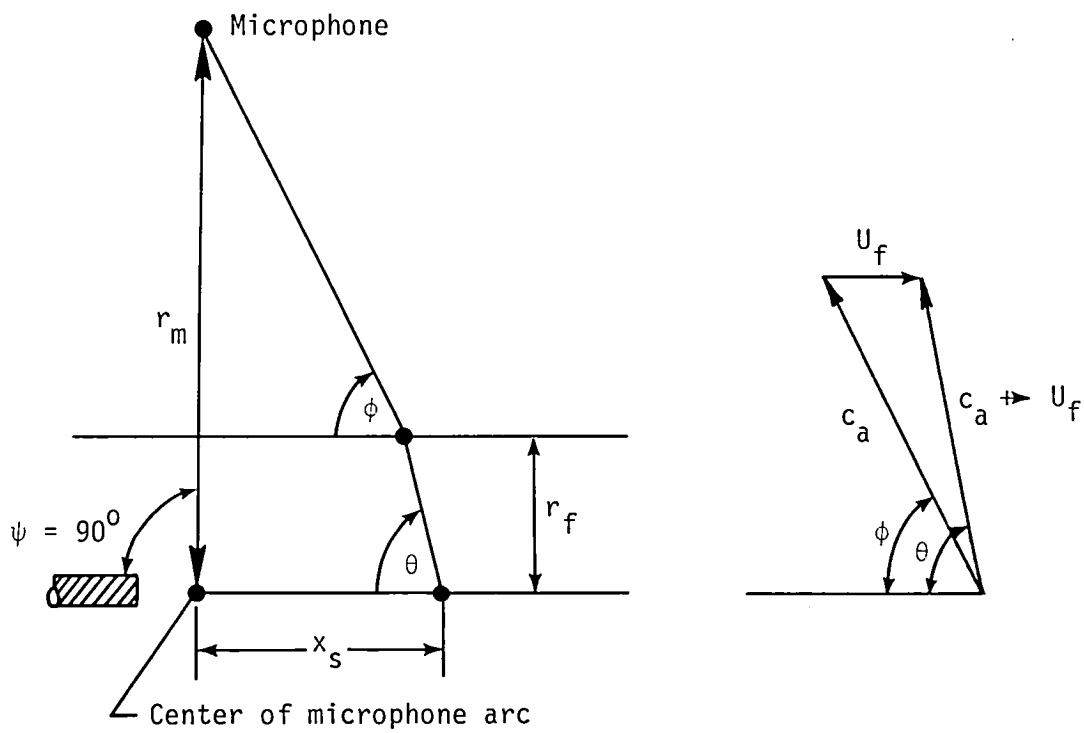

Figure 22.- Phase difference of broadband shock noise due to lack of far-field conditions.

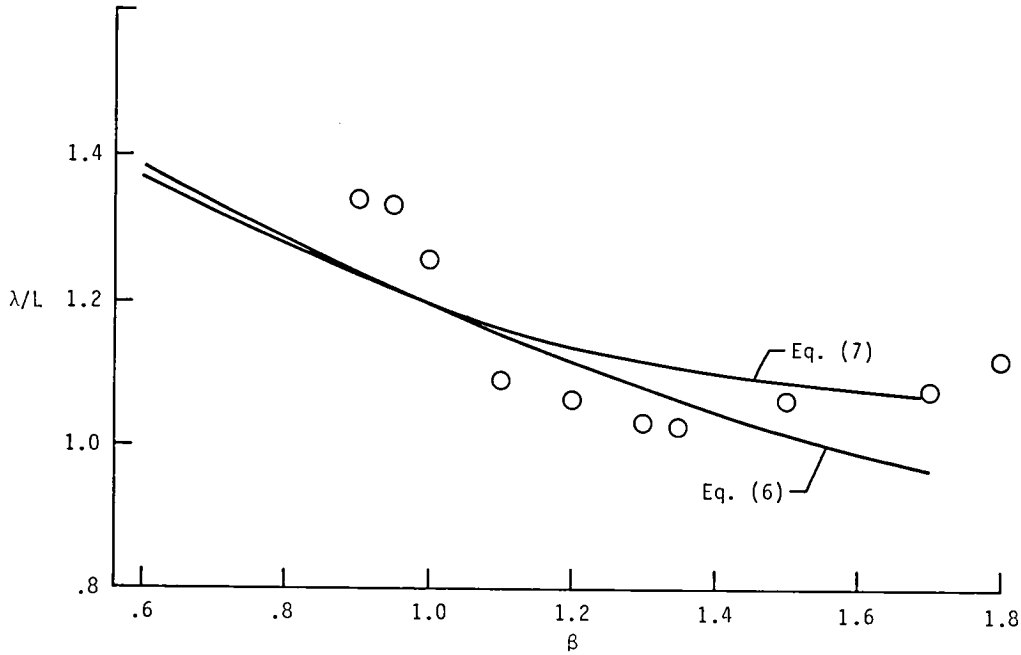

Figure 23.- Ratio of peak wavelength of broadband shock noise to shock spacing at static condition.

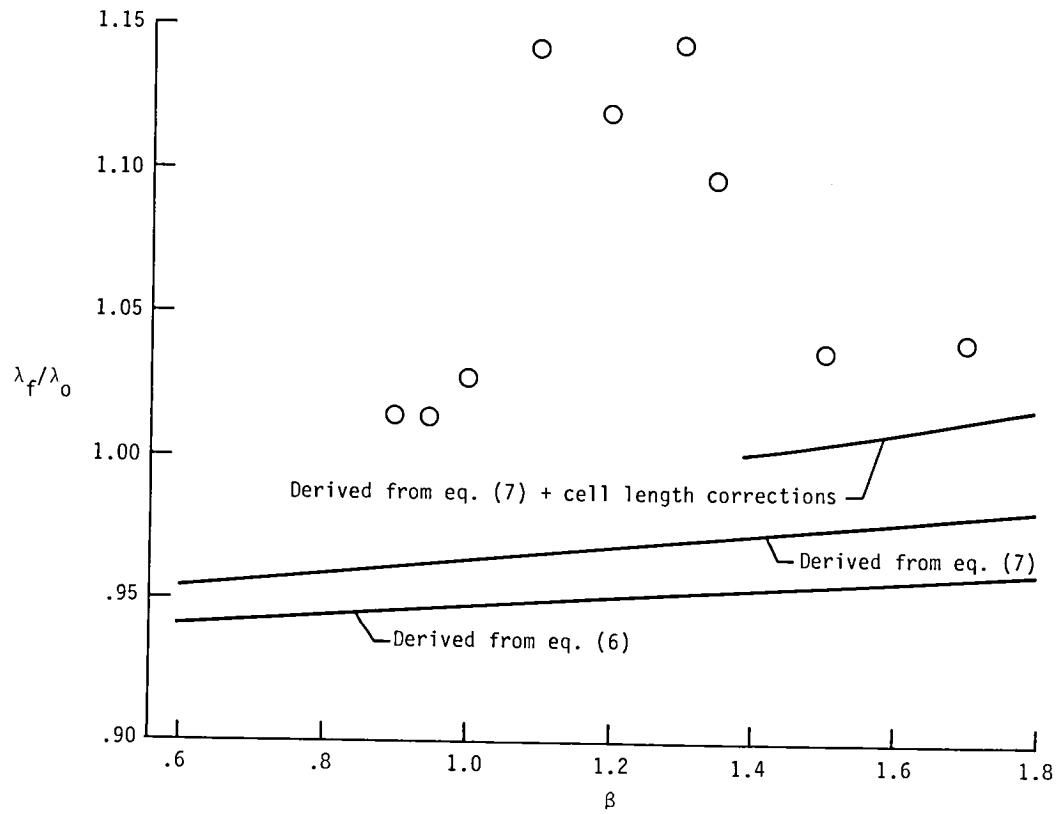

Figure 24.- Ratio of flight wavelength to static wavelength of broadband shock noise peak frequency.

1. Report No.	2. Government Accession No.	3. Recipient's Catalog No.
NASA TP-2308		

4. Title and Subtitle	5. Report Date
EFFECTS OF SIMULATED FLIGHT ON THE STRUCTURE AND NOISE OF UNDEREXPANDED JETS	May 1984
	6. Performing Organization Code: 505-31-33-12
7. Author(s): Thomas D. Norum and John G. Shearin	8. Performing Organization Report No.: L-15760
	10. Work Unit No.
9. Performing Organization Name and Address: NASA Langley Research Center, Hampton, VA 23665	11. Contract or Grant No.
	13. Type of Report and Period Covered: Technical Paper
12. Sponsoring Agency Name and Address: National Aeronautics and Space Administration, Washington, DC 20546	14. Sponsoring Agency Code

15. Supplementary Notes

16. Abstract

Mean plume static and pitot pressures and far-field acoustic pressure were measured for an underexpanded convergent nozzle in simulated flight. Results show that supersonic jet mixing noise behaves in flight in the same way that subsonic jet mixing noise does. Regarding shock-associated noise, the frequencies of both screech and peak broadband shock noise were found to decrease with flight speed. The external flow determines the dominant screech mode over a wide range of nozzle pressure ratios. Change in the screech mode strongly affects both the development of the downstream shock structure and the characteristic frequency of the broadband shock-associated noise. When no mode change occurs, the main effect of the external flow is to stretch the axial development of the shock cells.

17. Key Words (Suggested by Author(s))	18. Distribution Statement
Supersonic jet plume pressure Supersonic jet noise Shock noise Forward speed effects	Unclassified - Unlimited Subject Category 71

19. Security Classif. (of this report)	20. Security Classif. (of this page)	21. No. of Pages	22. Price
Unclassified	Unclassified	30	A03

For sale by the National Technical Information Service, Springfield, Virginia 22161

NASA-Langley, 1984

DO NOT REMOVE SLIP FROM MATERIAL

Delete your name from this slip when returning material to the library.

NAME	DATE	MS
Bhat, T.	2/9/93	165

NASA Langley (Rev. Dec. 1991) RIAD N-75